Quantitative assessment of parametric uncertainty in Northern Hemisphere PAH concentrations

Colin P. Thackray*[1], Carey L. Friedman[2], Yanxu Zhang[3] and Noelle E. Selin[4]

[1][Department of Earth, Atmospheric and Planetary Science, Massachusetts Institute of Technology, Cambridge, Massachusetts]

[2][Department of Earth, Atmospheric and Planetary Science and Center for Global Change Science, Massachusetts Institute of Technology, Cambridge, Massachusetts]

[3][School of Engineering and Applied Sciences, Harvard University, Cambridge, Massachusetts]

[4][Engineering Systems Division and Department of Earth, Atmospheric and Planetary Science, Massachusetts Institute of Technology, Cambridge, Massachusetts]

*Correspondence to:
C. P. Thackray (thackray@mit.edu), Telephone: 857-250-5183
77 Massachusetts Avenue 54-1810, Cambridge, MA, 02139, USA

TOC/Abstract Art:

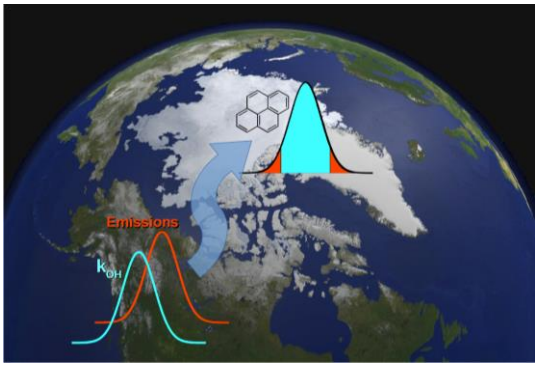

ABSTRACT

We quantitatively examine the relative importance of uncertainty in emissions and physicochemical properties (including reaction rate constants) to Northern Hemisphere (NH) and Arctic polycyclic aromatic hydrocarbon (PAH) concentrations, using a computationally-efficient numerical uncertainty technique applied to the global-scale chemical transport model GEOS-Chem. Using polynomial chaos (PC) methods, we propagate uncertainties in physicochemical properties and emissions for the PAHs benzo[a]pyrene, pyrene and phenanthrene to simulated spatially-resolved concentration uncertainties. We find that the leading contributors to parametric uncertainty in simulated concentrations are the black carbon-air partition coefficient and oxidation rate constant for benzo[a]pyrene, and the oxidation rate constants for phenanthrene and pyrene. NH geometric average concentrations are more sensitive to uncertainty in the atmospheric lifetime than to emissions rate. We use the PC expansions and measurement data to constrain parameter uncertainty distributions to observations. This narrows *a priori* parameter uncertainty distributions for phenanthrene and pyrene, and leads to higher values for OH oxidation rate constants and lower values for European PHE emission rates.

INTRODUCTION

Polycyclic aromatic hydrocarbons (PAHs) are mutagenic and carcinogenic environmental contaminants[1]. As persistent organic pollutants (POPs) that are transported through the atmosphere across national boundaries after emission, PAHs are regulated internationally by the Convention on Long-Range Trans-boundary Air Pollution (CLRTAP)[2]. Despite regulatory efforts, PAHs continue to be transported via the atmosphere to the Arctic[3–6], far from source regions. In this study, we quantitatively examine the relative importance of emissions and physicochemical parametric uncertainty to Northern Hemispheric (NH) and Arctic PAH concentrations, using efficient numerical uncertainty techniques applied to the global-scale chemical transport model (CTM) GEOS-Chem.

The pathways by which PAHs reach the Arctic have been studied with numerical models of varying complexity[7–13]. However, our understanding of these pathways is limited by substantial uncertainty associated with the physicochemical parameters (including reaction rate constants, partition coefficients and energies of phase change) that govern the atmospheric fate of PAHs. Some physicochemical parameters representing PAH behavior, such as oxidation rate constants and black carbon partition coefficients, are poorly constrained by measurements or several have not been measured directly[14–16]. For some PAHs, e.g. phenanthrene (PHE; three ring), physicochemical parameters important to their atmospheric fate have been relatively more studied than for the larger PAHs like benzo[a]pyrene (BaP; five ring) and pyrene (PYR; four ring). Even for PHE, measurements of physicochemical parameters can differ by more than a factor of two[15]. Limited knowledge of emissions sources and associated uncertainty also

63 contributes to uncertainty in atmospheric transport, as emissions factors for some processes (e.g.
64 waste incineration, biomass burning) can vary by orders of magnitude[17].

65 Model uncertainty has been studied for multimedia fate models of persistent organics[18–
66 20]. Multimedia model analyses have found that chemical properties have a larger influence on
67 persistence and long-range transport potential than model parameters such as spatial scales,
68 media heights/depths, and land and water surface fractions[18]. Detailed Monte Carlo analyses
69 have been performed for multimedia models, finding that emissions and degradation constants
70 were the most influential sources of uncertainty in DDT concentrations[19] and that partition
71 coefficients and reaction rate constants accounted for more than half of the uncertainty in
72 mercury concentrations in air and the surface ocean[21].

73 PAHs have been studied using finer-scale models at both the global and regional
74 scales[7,12,13,22,23]. Through comparison to spatially and temporally fine-scale measurements, these
75 studies show that highly spatially resolved models can be useful in predicting the pattern of
76 exposure to PAHs, an important factor for human health impacts. While multimedia models are
77 computationally efficient and thus can quantitatively examine relative influences of parameters
78 on uncertainty, they lack the spatial resolution and ability that CTMs possess to resolve the
79 episodic nature of atmospheric transport.

80 Monte Carlo-type methods like those used for multimedia models[19] can be prohibitively
81 computationally expensive for more finely spatially resolved models, as they require on the order
82 of thousands of samples for detailed analyses. Individual simulations run with complex
83 atmospheric CTMs such as GEOS-Chem can require hours to days of computational time,
84 leading to years for the full Monte Carlo analysis. Thus, first-order parameter sensitivity tests are

often used to characterize uncertainty in spatially resolved models[12,23,24].

One previous study[24] reported quantitative estimates of the relative importance of physicochemical parameter uncertainty and emissions uncertainty in PCB153 and α-HCH simulations by the large-scale, spatially-resolved (15°x15°) *BETR Research* model using a first-order error propagation method. Though first-order error propagation methods are computationally cheaper than Monte Carlo analysis, they do not directly quantify the effect of parameter uncertainty interactions. Polynomial chaos (PC)-based methods can greatly reduce the computational cost of uncertainty propagation for CTMs compared to Monte Carlo methods, while approximating the resulting uncertainty distributions more closely than first-order methods by extending to higher order. Parametric uncertainty in complex chemical mechanisms has been quantified using PC methods in a number of applications[25–28]. PC-based methods quantify the relative importance of each parameter, as well as account for their interactions in the model system, a significant advantage over traditional model parameter sensitivity tests. They also provide computational efficiency while retaining the spatial and temporal fidelity of CTMs.

We present here a first application of PC-based methods to a global atmospheric CTM of POPs. We use this analysis to quantify the contributions of emissions and physicochemical parameter uncertainty to NH- and Arctic-average concentrations of PHE, PYR, and BaP. We then combine the results of our PC analysis with measurements from long-term observation sites to constrain the values of these parameters.

METHODS

To quantify uncertainty in the GEOS-Chem PAH simulations, we compare simulated concentrations and associated uncertainties to measurements at non-urban sites, and use these

measurements and their uncertainties in a Bayesian analysis to constrain the probability distributions of the physicochemical parameters. Throughout this work we will refer to model "parametric uncertainty", which is the uncertainty in simulated concentrations resulting directly from the uncertainty in the model input parameters; i.e. physicochemical properties and emissions magnitudes.

GEOS-Chem Model

The simulations we assess in this study are carried out using the GEOS-Chem PAH chemical transport model[12]. This model has been used in previous studies to simulate long-range atmospheric transport of PAHs and has allowed comparison to measurements where it has been able to resolve meteorologically-driven episodic high-concentration events[12]. Evaluation of the model against measurements in both mid-latitudes and the Arctic, and traditional sensitivity tests have been conducted previously; we refer the reader to the referenced papers for a detailed assessment of model perfomance[12,13]. Here, we briefly describe major features of the model, including meteorology, emissions, chemistry, and gas-particle partitioning. GEOS-Chem uses assimilated meteorology from the NASA Goddard Earth Observing System's GEOS-5 dataset at a temporal resolution of 6 hours, a horizontal resolution of 0.5º x 0.667º re-gridded to 4º x 5º for computational efficiency, and 47 levels vertically. The simulations for this study were run for the years 2006-2008. PAH emissions in the model come from the inventory of Zhang and Tao[17], which represents annual emissions from the year 2004, is resolved on the national scale, and includes details for individual sectors and PAHs but is not time-resolved, meaning the emissions are not seasonally or annually varying. Emissions are discussed in more detail in following sections. Each model run begins with a "spin-up" period of one simulated year to negate the transient effects of initial conditions.

Upon emission, the model partitions PAHs between the gas and aerosol phases using a black carbon-air partition coefficient (K_{BC}) to represent partitioning to black carbon (BC) aerosol and an octanol-air partition coefficient (K_{OA}) to represent partitioning to organic carbon (OC). The overall gas-particle partitioning is governed by a dual OC absorption and BC adsorption model[12] based on the Dachs-Eisenreich[29] equation. Both OC and BC concentrations are prescribed as monthly averages in the PAH simulations, pre-calculated from full chemistry GEOS-Chem simulations[10,30] for computational efficiency. Gas-particle partitioning is re-calculated at each chemistry time step of GEOS-Chem (60 min). The effect of using this coarse time resolution of prescribed particle concentrations was found to be small compared to the parametric uncertainties discussed below[13].

Each of these partition coefficients' temperature dependence is determined by an internal energy of phase change according to the van't Hoff relationship. These internal energies are governed by enthalpies of phase change. The enthalpy of vaporization ΔH_{vap} is the uncertain parameter that determines the sensitivity of particle partitioning to changing temperature, while the enthalpy of solvation in liquid water ΔH_{sol} in combination with ΔH_{vap} determines that of wet deposition.

We simulate the oxidation of gas phase PAHs by reaction with hydroxyl radicals (OH). Monthly average OH concentrations are prescribed by a GEOS-Chem full chemistry simulation[31] with a daily cycle overlaid on these monthly averages. PAH reaction with OH is represented by a second order reaction with reaction rate constant k_{OH}. On-particle oxidation by ozone is simulated using the parametrization of Kahan et al.[32]

Both gas- and particle-phase PAHs undergo wet deposition in the simulations. Gas-phase

PAH is scavenged by liquid water according to the air-water partitioning coefficient K_{AW}, which is temperature dependent according to ΔH_{AW} (a combination of ΔH_{sol} and ΔH_{vap}) following the van't Hoff relationship. Dry deposition for gas-phase PAH is simulated according to Wang et al.[33], with lipophilic uptake scaled by the K_{OA} [12]. A complete evaluation of GEOS-Chem simulations of PAHs can be found in the original work by Friedman and Selin[12]. The seven uncertain physicochemical parameters mentioned above are included in our analysis for each PAH.

Polynomial chaos

The PC-based estimator uses orthogonal polynomials to approximate GEOS-Chem model output as a function of model inputs. The polynomial expansion of the model output to be estimated takes the form

$$\eta(\xi) = \alpha_0 + \sum_{j=1}^{d}\sum_{k=1}^{M} \alpha_{j,k} H_j(\xi_k) + \sum_{k=1}^{M-1}\sum_{l=k+1}^{M} \beta_{k,l} H_1(\xi_k)H_1(\xi_l) + \cdots + Order(d) \quad (1)$$

where the estimator η of degree d is a function of the polynomials H_j of order j, the M variables ξ_k representing model inputs, the expansion coefficients $\alpha_{j,k}$ and $\beta_{k,l}$, and higher order coefficients. The terms not shown in the equation are cross terms of degree greater than two, which include the product of up to d Hermite polynomials of different variables, analogous to the second order cross terms shown. In this study, we truncate the polynomial after third order. To obtain the expansion coefficients, one model run at a unique set of inputs is performed for each term in equation (1)[34]. The set of inputs for the model runs for each degree's terms are the values corresponding to the roots of the next degree's polynomials. The outputs of these model runs and the corresponding sets of input values are used to set up a system of equations to solve

for the expansion coefficients[27]. Further description, along with validation, of the PC expansion can be found in the Supporting Information (section S4).

We use the polynomial estimator to directly infer properties of the uncertainty distribution of model output (in this case total (gas plus particulate phase) PAH mass concentration) without relying on Monte Carlo methods, which is accomplished using the analytical forms of the mean, variance and skewness from the polynomial coefficients[27]. We also calculate the portion of the total output variance contributed by each input parameter using the expansion coefficients[27,28].

Physicochemical parameter uncertainties

We conduct an extensive review of the literature for experimentally determined values of each of seven uncertain physicochemical parameters for the three PAHs investigated in this study, and construct probability distributions based on the available data (summarized in Tables S1-S3). The distributions (Table 1 and discussed below), are for the parameters that most directly affect the simulated atmospheric fate and transport of the PAHs based on previously-conducted traditional model sensitivity testing[12]. Model processes that are sources of uncertainty for all chemicals (including non-POPs) simulated by GEOS-Chem, such as advection and wet deposition schemes, are not the focus of this study.

Partition coefficients (air-water: K_{AW}, black carbon-air: K_{BC}, octanol-air: K_{OA}): Since the partition coefficients used in the model are experimentally determined and reported in log form, we estimate their uncertainty distributions as normal distributions of the log values,

with the means and standard deviations derived from literature values (see SI for details and references).

K_{BC}, which describes the fraction of PAH found in the BC phase given an amount of BC particulate matter, is the combination of K_{AW} and the BC-water partition coefficient ($K_{BC\text{-}Water}$)[35],

$$\log(K_{BC}) = -\log(K_{AW}) + \log(K_{BC-Water}) \quad (2)$$

where $K_{BC\text{-}Water}$ gives the ratio of concentrations of PAH in the BC particulate phase to dissolved PAH at equilibrium. Since K_{BC} itself is not an independent parameter due to its relationship to K_{AW}, we use the independent $K_{BC\text{-}Water}$ instead as the uncertain parameter for this study.

Enthalpies of phase change (ΔH_{vap} and ΔH_{sol}): We estimate the uncertainty distributions for the enthalpy of vaporization (ΔH_{vap}) and the enthalpy of solvation (ΔH_{sol}) for PHE, PYR and BaP as normal distributions with the means and standard deviations of a collection of literature values of ΔH_{vap} or ΔH_{sol} for each PAH (see SI for details and references).

On-particle ozone oxidation rate constant (k_{O3}): For all three PAHs, we use the reported "A" and "B" kinetic parameter values and their uncertainties from Kahan et al.[32] as model inputs. Across all atmospheric ozone concentrations, the B-parameter dominates the contribution to uncertainty in k_{O3}, so we neglect A-parameter uncertainty in our analysis.

OH oxidation rate constant (k_{OH}): For PHE, we estimate the uncertainty distribution from three literature values and their associated uncertainties[14,36,37]. The mean value of the normal uncertainty distribution is estimated by the uncertainty-weighted mean of these three values, and the standard deviation of the distribution is estimated by the standard deviation of the weighted mean.

While there is no literature value for BaP's or PYR's k_{OH}, values can be obtained from

214 the Atmospheric Oxidation Program software AOPWIN, which uses an ionization potential-
215 activity relationship[38],

$$\ln(k_{OH}) = -4.345 - 2.494(IP) \quad (3)$$

216 where k_{OH} has units of cm^3 $molec^{-1}$ s^{-1} and IP is the ionization potential in units of eV.

217 We use the mean and standard deviation of the National Institute of Standards and
218 Technology collection of reported ionization potentials for BaP[39] to estimate a normal
219 distribution that results in a log-normal distribution of IP-derived k_{OH} values. Similarly, for PYR
220 we use the mean and standard deviation of the collection of reported PYR IPs[40] to estimate the
221 uncertainty distribution for PYR's k_{OH}.

222 **Regional emissions uncertainties**

223 Emissions uncertainty results from uncertainties in both emission activities (quantity of a
224 given type of emitting process) and emission factors (PAH emission quantity per activity). The
225 total PAH emission *E* due to a process *i* can be divided into those two elements:

$$E_i = A_i F_i \quad (4)$$

226 where A_i is the emissions activity of process *i* and F_i is the emission factor for that process. F_i
227 can be uncertain to a much larger degree than A_i [17] because the conditions under which each
228 emitting process is carried out in reality are highly varying but summarized by a single value.
229 Measurements of F_i of the same process by different experimenters can yield orders of
230 magnitude differences[17]. For example, F_i associated with diesel fuel in the transport sector will
231 depend on such factors as the type of fuel burned, type of engine burning the fuel, and
232 temperature and condition of the engine. PAH emissions processes with the largest uncertainties

in F_i include primary aluminum production, use of traffic gasoline, diesel, and kerosene, industrial coal burning, and non-transport petroleum combustion[17].

Given that there are distinct source contributions to PAH emissions and their uncertainties in different regions of the globe, we define discrete emissions regions, and calculate an *a priori* probability distribution for the total emissions of each region. We choose the regions of North America, Europe, South Asia, East Asia and Africa because of the large magnitude of emissions (South Asia, East Asia, Africa), and proximity to the Arctic (North America and Europe). We estimate the uncertainty distribution of total emissions of each region using Monte Carlo sampling over each country's A_i and the F_i uncertainty distributions[17] and assume that the spatial distribution of emissions within each region remains fixed. Regional emission distributions (Figures S1-S3) are then used as input parameters, along with physicochemical parameters, in the above-described PC analysis.

In-situ observations

We use observed annual average total (gas+particulate) BaP, PYR, and PHE concentrations from each of 10 sites monitored by the Co-operative Programme for Monitoring and Evaluation of the Long-range Transmission of Air Pollutants in Europe (EMEP), Integrated Atmospheric Deposition Network (IADN), and Environment Canada (EC) observation networks in the Northern Hemisphere (NH) for comparison to model values. All observations were collected at land-based non-urban sites using high-volume air samplers. Particle-bound PAHs were collected on glass fibre filters, and volatile PAHs were adsorbed to polyurethane foam (PUF) plugs. Spatial coverage includes the Great Lakes, Northern Europe, and two Arctic sites. Site locations, concentrations and references are summarized in Table S4, and are the same sites

used for model-measurement comparison by Friedman and Selin[12].

For site-by-site comparison to simulated concentrations, we calculate observational errors following Chen and Prinn[41]. The observational error for comparison to a model grid box accounts for statistical representativeness (accounting for some stations' non-continuous sampling), analytical method precision error, site inter-calibration error, and spatial mismatch error (i.e. a single point's representativeness of the whole grid-box). These errors (see Table S4) represent the variability in observed values that is impossible to capture with any model, and are thus separate from model uncertainty. These errors range from ±25% to a factor of 3, depending on the measurement site and the PAH in question.

Constraint of physicochemical parameters by observations

Using the annual average measurements outlined above, and PC-estimated concentrations based on annual average model output, we constrain the physicochemical parameter uncertainty distributions by Bayesian inference, combining information from observations and *a priori* parameter uncertainties. We compare 1) the PC polynomial-estimated concentration in the model grid box encompassing a measurement location for a given set of physicochemical and emissions parameter values to 2) the observed concentration at the same location. By mapping the predicted concentrations as a function of the uncertain parameters using the PC estimator, we define a weighted least-squares cost function of the form:

$$K(\xi)^2 = \sum_{i=1}^{N} \left(\frac{Y_i - \eta_i(\xi)}{\sigma_i} \right)^2 \quad (5)$$

where summation is over the N measurement locations, Y_i is the observed value at a particular site, $\eta_i(\xi)$ is the polynomial estimate at parameter values ξ, and σ_i is the total "observation

errors" from above at measurement site i.

With the least-squares comparison above, the likelihood function $P(Y|\xi)$ is related to the cost function via

$$P(Y|\xi) \propto e^{-K(\xi)^2}. \quad (6)$$

This makes use of the PC estimators and the site measurements and their errors to estimate the likelihood of observing the concentrations Y as a function of the parameter values ξ.

To update the *a priori* uncertainty distributions, we use Bayes' rule for the *a posteriori* distribution $P(\xi|Y)$:

$$P(\xi|Y) \propto P(\xi)P(Y|\xi) \quad (7)$$

where $P(\xi)$ is the prior uncertainty distribution. This results in a description of the relative probabilities of each physicochemical parameter value, given the available constraining measurements.

RESULTS

We calculate polynomial estimators as described above, and evaluate their predicted log-concentrations against independent full GEOS-Chem model runs. Over the parameter space covered by the physicochemical property uncertainty distributions, the polynomial estimator

matches the validation data-set with r^2 greater than 0.99 (see Figure S4) for all three PAHs. We use the polynomial estimators to calculate model uncertainty distributions for NH and Arctic (above 66°N) surface concentration geometric averages for annual and Northern Hemisphere winter (DJF) and summer (JJA) periods for all three PAHs, attribute fractions of this uncertainty to individual model parameters, and constrain parameter uncertainty distributions using observation site data.

Comparison to measurements

Figure 1 shows a comparison of monthly average concentrations simulated using the PC-based estimator and associated parametric uncertainties to measured average concentrations and measurement uncertainties for non-urban sites for each PAH. The simulations capture the measurements within the ±2σ parametric uncertainty interval for all three PAHs, with PYR and BaP capturing the measurement means within the ±σ interval.

Simulated PHE concentrations show agreement with measurements during the winter-spring and summer-fall transitions, but measured means are higher than simulated during JJA and lower during DJF[12]. In the summer, the measured mean falls within the ±σ bounds of the model, but during the winter months (Nov, Dec, Jan, Feb), the measured concentrations fall between the –σ and -2σ model values. This discrepancy could be due to unresolved seasonality of emissions, or secondary sources which are not represented in the simulations, but have been tested and discussed previously[13]. PYR simulated concentrations are lower than observed concentrations for all except the winter months. The observed values do, however, fall into the ±σ range of the model uncertainty distribution for all months. BaP simulated concentrations have the highest parametric uncertainty, and the observed concentrations fall into the ±σ range of

the model for all months of the year, with the simulated seasonal cycle following the observed cycle closely.

Northern Hemisphere and Arctic model uncertainty in concentration

Figure S5 shows model parametric uncertainty distributions for BaP, PYR and PHE, for both NH and Arctic average concentrations, and for annual, winter, and summer temporal averages. Across all three PAHs, JJA average simulated concentrations are lower with higher uncertainty than DJF averages. PHE concentrations have the least parametric uncertainty, with a range (95% confidence interval) spanning approximately one order of magnitude for annual, summer, and winter averages. PYR and BaP parametric uncertainty ranges during the summer span more than two orders of magnitude, and close to an order of magnitude during the winter.

In the Arctic, parametric uncertainty is at its lowest for all three PAHs during the winter, when there is little to no sunlight to drive photochemical oxidation. Average concentrations of PAHs are highest during the winter, and lowest during the summer in the Arctic because of the presence of OH for oxidation, and this relative abundance of OH also drives the sensitivity of the PAH concentrations to oxidation rate constant uncertainty. The seasonal difference in the Arctic average PAH concentration is more pronounced than the NH average, with summer-winter differences for all three PAHs of more than three orders of magnitude.

Contributors to model parametric uncertainty

The important sources of model parametric uncertainty are substantially different between NH and Arctic average concentrations, and across the three PAHs. Table S5 shows the fractional contribution of leading parameters to the total resulting model parametric concentration uncertainty for PHE, PYR, and BaP. Figures S10-S20 show the spatial

distributions of these contributions across the globe.

At the hemispheric scale, PHE concentration parametric uncertainty is driven year-round by uncertainty in the oxidation rate constant. Since PHE is mostly in the gas phase (90%-100% [12]), uncertainty in its gas-phase lifetime is the most important contributor to parametric uncertainty in the NH average simulated concentrations. In the Arctic average, however, uncertainty in European emissions gains importance, contributing close to a third of the parametric uncertainty annually and 64% in the winter. The relative importance of emissions and reduced importance of oxidation rate constant uncertainty during Arctic winter is due to the lack of atmospheric OH radicals. During the summer, European emissions uncertainty remains a significant secondary contributor, but k_{OH} uncertainty makes up the largest fraction of the total for the model.

The contributors of PYR parametric concentration uncertainty follow a similar pattern to those of PHE. Because of the large uncertainty in the oxidation rate constant for PYR (see Table 1) and the fact that >50% of atmospheric PYR is in the gas phase[12], the parametric concentration uncertainty in the NH annual average is dominated by uncertainty in k_{OH}. Like for PHE, the second-most important contributor to parametric uncertainty is European emissions.

BaP has the most varied contributions of the three PAHs studied. For the NH annual average, uncertainty in $K_{BC\text{-}Water}$ contributes 63% of the total uncertainty, with k_{OH} uncertainty contributing 30%, and the uncertainty in ΔH_{vap}, European, and North American emissions making up the other 7%. This behavior changes little between the winter and summer season.

In the Arctic, $K_{BC\text{-}Water}$ is the leading source of parametric uncertainty for BaP. It contributes 55% annually, while k_{OH} contributes 35% and 6% is due to ΔH_{vap}. During the

358 relatively photochemistry-free winter months, the contribution from k_{OH} drops to 3%, and the
359 difference is made up by increases in the contributions of ΔH_{vap} (to 11%), and European
360 emissions (to 29%). In the summer, the opposite occurs and k_{OH} uncertainty contributes 52% of
361 the total.

362 Across all three PAHs, the contribution of physicochemical parameter uncertainty makes
363 up more than 94% of the NH average parametric uncertainty. This is because a large fraction of
364 the globe is far from emission sources, so wide spatial average concentrations are more sensitive
365 to the uncertainty in the atmospheric lifetime than they are to emissions magnitude. In the case of
366 PYR, parametric uncertainty in the atmospheric lifetime is almost entirely due to uncertainty in
367 the oxidation rate because of the extremely high uncertainty in oxidation rate constant. For PHE,
368 k_{OH} also contributes most to uncertainty because PHE is mostly found in the gas phase. In the
369 case of BaP, the uncertainty in the atmospheric lifetime is due to both the highly uncertain gas
370 phase oxidation rate, but also the amount of BaP found in the particulate phase, which is
371 primarily controlled by BC partitioning. Because of its nature as a mostly particulate matter-
372 bound PAH, BaP uncertainty has a larger contribution from the uncertainty in $K_{BC\text{-}Water}$ and
373 ΔH_{vap}, which together control partitioning to BC.

374 Closest to each emissions source region, uncertainty in that region's emissions becomes
375 most import, as removal during transport has not had time to take effect. Europe is the region
376 with sources closest to the Arctic, and therefore European emissions uncertainty contributes
377 more to simulated Arctic concentration uncertainty than other regional emissions. The emissions
378 uncertainty contribution reaches a maximum during the winter, when concentrations of all three
379 PAHs are highest due to lower loss rates, making it an important factor in the quantification of
380 PAH transport to the Arctic.

381 **Observation-constrained parameter distributions**

382 We constrain the probability distributions of parameter values using the spatially
383 distributed modeled and observed concentrations as described in the Methods section. Figure 2
384 shows the observation-derived likelihood distributions, and prior and posterior probability
385 distributions of the two most important parameters for model uncertainty at the measurement
386 sites. PHE's and PYR's leading parameters are constrained by the analysis, while BaP's are
387 effectively unconstrained.

388 As shown in Figure 2(a), for PHE, the highest observation-constrained likelihood comes
389 when k_{OH} is highest and the European regional emission rate is low. The result is that the
390 posterior distributions for k_{OH} and E_{Europe} have maximums at higher and lower values,
391 respectively. Figure 2(b) shows a similar constraining effect of the observations for PYR's k_{OH},
392 which is shifted higher, while the E_{Europe} posterior distribution is narrowed around the same value
393 as the prior distribution. Figure 2(c) shows that the measurement comparison added no
394 constraints to the prior parameter distributions for BaP (neither confirming nor denying the
395 assumed prior), due to the larger uncertainties in both its simulated and observed concentrations.

396 After constraint by the measurement data, we estimate new most likely values for PYR's
397 and PHE's k_{OH} and rate of emission in Europe. The *a priori* best estimate of k_{OH} for PYR was
398 $7x10^{-11}$ $cm^{-3}s^{-1}$, while the updated best estimate is $1x10^{-10}$ $cm^{-3}s^{-1}$. The prior estimate of k_{OH} for
399 PHE of $1.9x10^{-11}$ $cm^{-3}s^{-1}$ is updated to $2.3x10^{-11}$ $cm^{-3}s^{-1}$. We lower our best estimates of European
400 emissions for PHE from 5.8 kt/yr to 4.1 kt/yr.

401

402

DISCUSSION

Through the uncertainty attribution described above, we identify the key parameters for which reducing uncertainty would improve our ability to model long-range transport of PAHs. For PHE and PYR, k_{OH} uncertainty has the largest impact on model results, while for BaP k_{OH}, $K_{BC\text{-}Water}$, and ΔH_{vap} all contribute to uncertainty in simulated concentrations. These results are similar to findings for multimedia models of other environmental toxics, which indicate that degradation rates and partition coefficients are the largest contributors to parametric uncertainty[19,21]. Across all three PAHs, more precise experimental quantification of k_{OH} could greatly reduce parametric model uncertainty. In particular for PYR and BaP, the lack of experimental values of k_{OH} leads to an additional step in the propagation of uncertainty, as the value of k_{OH} used in the model is itself a parametrization. With reduced k_{OH} uncertainty, we would be better able to constrain PAH emissions using observations of concentrations, and we would improve our ability to use modeling to inform policy[42].

We are able to quantitatively attribute simulated concentration uncertainty to individual model parameters while accounting for non-linear model responses in a computationally efficient manner. Because of the method's relatively low number of required model runs, it could be applied to other spatially resolved environmental models for low-cost but detailed identification of leading contributors to parametric uncertainty. The detailed parametric uncertainty analysis that this method provides is an important aspect of environmental transport model simulations that is commonly unreported in the literature. This type of analysis should be carried out for other substances and models, as the conclusions from our simulations of PAHs specifically may not apply to other substances or models. This is evident in comparison to the first-order uncertainty analysis for *BETR Research* PCB153 simulations[24], which suggests that emissions

426 uncertainties account for more than 90% of the simulated atmospheric concentration parametric
427 uncertainty under current climate and emissions.

428 We constrain physicochemical and emissions parameters using measurements, with
429 updated uncertainty distributions for k_{OH} and E_{Europe} for PHE and PYR. While this method
430 represents a quantitative improvement over traditional model sensitivity tests, in which
431 parameters are altered based on forward matches to observations, our approach also has
432 important limitations. The constraint relies on the comparison of concentrations measured at a
433 point to the average concentration within a GEOS-Chem grid-box. While we account for this
434 through an estimate of representativeness error, spatial heterogeneities within the grid-box are
435 not represented and could introduce an unquantified bias in the comparisons due to this
436 mismatch of spatial resolutions. We do not optimize for the spatial distribution of emissions in
437 this study, which precludes the ability to account for a local emission source that could be
438 driving observed concentrations at a site. Our analysis also relies on the quantification of the
439 emissions parameters and their uncertainty at the inventory's national level, and any potential
440 biases in these estimates would propagate to our results. For example, an underestimation of the
441 uncertainty in biomass burning emissions factors in the inventory would propagate through the
442 model to result in an underestimate of concentration uncertainty.

443 While we quantify the impact of uncertainties in regional emission magnitudes and
444 physicochemical properties on simulated concentrations in detail, there are other sources of
445 uncertainty in simulated concentrations. Emissions can vary substantially temporally, and on
446 spatial scales finer than those considered here. These temporal and spatial resolution mismatches
447 between the simulations and reality will have a more limited effect on large spatial and time
448 averages than on shorter-term localised concentrations. Along with direct emissions, secondary

449 emissions (revolatilization) from surface media can affect atmospheric PAH concentrations, and
450 these secondary sources are not resolved in this work. The accuracy and time-resolution of
451 prescribed concentrations of particulate matter and OH used in the model can also introduce
452 uncertainty, but this uncertainty is significantly smaller than that due to their associated chemical
453 parameters[13]. There is also non-parametric uncertainty associated with the particle partitioning
454 scheme used, as deviations from measurements can be large, especially for smaller PAHs[15]
455 whose concentrations have lower sensitivity to particle partitioning. Theoretical issues have been
456 identified with the parametrization of partition coefficients[43], which we have not accounted for
457 here. Limitations of particle partitioning schemes for PAHs in GEOS-Chem have been
458 investigated in detail previously[23]. Considering these uncertainties, our results suggest that for
459 BaP, further constraints on partitioning properties would improve our ability to capture long-
460 range transport.

461 Chemical transport modeling is susceptible to a variety of sources of uncertainty that are
462 not unique to the simulation of PAHs. Advection in the atmosphere is carried out on a large scale
463 that is only representative of the actual advection in the atmosphere on a coarse scale. This
464 advection is based on meteorological reanalysis fields that have their own uncertainty. Prescribed
465 precipitation also contributes to uncertainty in wet deposition. However, many of these processes
466 in GEOS-Chem are evaluated and constrained using simulations of other atmospheric
467 constituents (e.g. carbon monoxide, ozone) for which measurement data are less uncertain and
468 more widely available[44–46]. The source of uncertainty most difficult to quantify is that which is
469 associated with PAH-specific processes not represented by the model (e.g. on-particle oxidation
470 reactions other than ozonation). A process that is not described by the model would not be
471 represented in a parametric uncertainty analysis, and depending on the importance of the process

472 could be a major source of unquantified uncertainty.

473 Based on model sensitivity (Figures S6-S9), the most effective locations for hypothetical
474 future measurement sites that could be used to improve the constraint of the most important PAH
475 physicochemical properties are far from sources and are generally in regions where wet
476 deposition is relatively less important, particularly in the Southern Hemisphere. These locations,
477 however, have very low PAH concentrations, below common quantification limits. The resulting
478 measurement constraint paradox is that the locations that would best constrain physicochemical
479 properties have concentrations that are the most difficult to measure. This means that greatly
480 reducing model parametric uncertainty by observational constraint will require very low
481 detection limits at long-term remote sites. Measuring these low concentrations is potentially
482 achievable for the gas phase using passive air samplers, which accumulate greater contaminant
483 mass over longer periods of time than traditional active samplers[42].

484 The results we present give important insight into the parametric uncertainty distributions
485 of simulated PAH concentrations and their relationship to specific inputs. Our analysis
486 demonstrates that there is a need to reduce the large parametric uncertainties stemming from
487 physicochemical property data for PAHs, and identifies the properties which contribute most to
488 model parametric uncertainty. While our analysis shows that long-term measurement sites can be
489 used to constrain physicochemical property values for PHE and PYR, highlighting the
490 importance of such measurements of atmospheric PAHs, better experimental quantification of
491 PAH properties would provide the greatest reductions in simulated concentration uncertainty.
492 We identify quantitatively which physicochemical properties of PHE, PYR and BaP could be
493 targeted experimentally to greatly reduce simulated concentration uncertainty.

SUPPORTING INFORMATION AVAILABLE

The supporting information includes physicochemical property data and associated uncertainties, emissions uncertainty information, measurement site info, data, and errors, seasonal parametric uncertainty comparisons, and parametric uncertainty contributions as a function of latitude and longitude. This information is available free of charge via the Internet at http://pubs.acs.org/.

ACKNOWLEDGMENTS

This work was supported by the U.S. National Science Foundation Arctic Natural Sciences Program (#1203526) and the Atmospheric Chemistry Program (#1053658). We thank Marta Venier and Ronald Hites (Indiana University) and Hayley Hung and the Northern Contaminants Program (Environment Canada) for observational data.

REFERENCES

(1) Boffetta, P.; Jourenkova, N.; Gustavsson, P. Cancer risk from occupational and environmental exposure to polycyclic aromatic hydrocarbons. *Cancer Causes Control* **1997**, *8* (3), 444–472.

(2) UNECE. *Protocol to the 1979 Convention on Long-Range Transboundary Air Pollution on Persistent Organic Pollutants*; United Nations Economic Commission for Europe, 1998.

(3) Halsall, C. J.; Barrie, L. A.; Fellin, P.; Muir, D. G. .; Billeck, B. N.; Lockhart, L.; Rovinsky, F.; Kononov, E.; Pastukhov, B. Spatial and temporal variation of polycyclic aromatic hydrocarbons in the Arctic atmosphere. *Env. Sci Technol* **1997**, *31*, 3593–3599.

(4) Macdonald, R. W.; Barrie, L. A.; Bidleman, T. F.; Diamond, M. L.; Gregor, D. J.; Semkin, R. G.; Strachan, W. M.; Li, Y. F.; Wania, F.; Alaee, M.; et al. Contaminants in the Canadian Arctic: 5 years of progress in understanding sources, occurrence and pathways. *Sci Total Env.* **2000**, *254* (2-3), 93–234.

(5) Halsall, C. J.; Sweetman, A. J.; Barrie, L. A.; Jones, K. C. Modelling the behaviour of PAHs during atmospheric transport from the UK to the Arctic. *Atmos Env.* **2001**, *35*, 255–267.

(6) Hung, H.; Blanchard, P.; Halsall, C. J.; Bidleman, T. F.; Stern, G. A.; Fellin, P.; Muir, D. C. G.; Barrie, L. A.; Jantunen, L. M.; Helm, P. A.; et al. Temporal and spatial variabilities of atmospheric polychlorinated biphenyls (PCBs), organochlorine (OC) pesticides and polycyclic aromatic hydrocarbons (PAHs) in the Canadian Arctic: Results from a decade of monitoring. *Sci. Total Environ.* **2005**, *342* (1-3), 119–144.

(7) Sehili, A. M.; Lammel, G. Global fate and distribution of polycyclic aromatic hydrocarbons emitted from Europe and Russia. *Atmos Env.* **2007**, *41*, 8301–8315.

(8) Wania, F.; Mackay, D. A global distribution model for persistent organic chemicals. *Sci Total Env.* **1995**, *161*, 211–232.

(9) Scheringer, M.; Wegmann, F.; Fenner, K.; Hungerbuhler, K. Investigation of the cold condensation of persistent organic pollutants with a global multimedia fate model. *Env. Sci Technol* **2000**, *34*, 1842–1850.

(10) Wang, Q.; Jacob, D. J.; Fisher, J. A.; Mao, J.; Leibensperger, E. M.; Carouge, C. C.; Le Sager, P.; Kondo, Y.; Jimenez, J. L.; Cubison, M. J.; et al. Sources of carbonaceous aerosols and deposited black carbon in the Arctic in winter-spring: implications for radiative forcing. *Atmos Chem Phys* **2011**, *11*, 12453–12473.

(11) Lammel, G.; Sehili, A. M.; Bond, T. C.; Feichter, J.; Grassl, H. Gas/particle partitioning and global distribution of polycyclic aromatic hydrocarbons- A modelling approach. *Chemosphere* **2009**, *76*, 98–106.

(12) Friedman, C. L.; Selin, N. E. Long-range atmospheric transport of polycyclic aromatic hydrocarbons: A global 3-D model analysis including evaluation of Arctic sources. *Env. Sci Technol* **2012**, *46*, 9501–9510.

(13) Friedman, C. L.; Zhang, Y.; Selin, N. E. Climate change and emissions impacts on atmospheric PAH transport to the Arctic. *Env. Sci Technol* **2014**, *48*, 429–437.

(14) Brubaker, W. W.; Hites, R. A. OH reaction kinetics of polycyclic aromatic hydrocarbons and polychlorinated dibenzo-p-dioxins and dibenzofurans. *J Phys Chem A* **1998**, *102*, 915–921.

(15) Lohmann, R.; Lammel, G. Adsorptive and absorptive contributions to the gas-particle partitioning of polycyclic aromatic hydrocarbons: State of knowledge and recommended

parametrization for modeling. *Env. Sci Technol* **2004**, *38*, 3793–3803.
(16) Shiu, W.-Y.; Ma, K.-C. Temperature dependence of physical-chemical properties of selected chemicals of environmental interest. I. Mononuclear and polynuclear aromatic hydrocarbons. *J Phys Chem Ref Data* **2000**, *29*, 41–130.
(17) Zhang, Y.; Tao, S. Global atmospheric emission inventory of polycyclic aromatic hydrocarbons (PAHs) for 2004. *Atmos Env.* **2009**, *43*, 812–819.
(18) Fenner, K.; Scheringer, M.; MacLeod, M.; Matthies, M.; McKone, T.; Stroebe, M.; Beyer, A.; Bonnell, M.; Le Gall, A. C.; Klasmeier, J.; et al. Comparing estimates of persistence and long-range transport potential among multimedia models. *Environ. Sci. Technol.* **2005**, *39* (7), 1932–1942.
(19) Schenker, U.; Scheringer, M.; Sohn, M. D.; Maddalena, R. L.; McKone, T. E.; Hungerbühler, K. Using information on uncertainty to improve environmental fate modeling: A case study on DDT. *Env. Sci Technol* **2009**, *43*, 128–134.
(20) Meyer, T.; Wania, F. What environmental fate processes have the strongest influence on a completely persistent organic chemical's accumulation in the Arctic? *Atmos Env.* **2007**, *41*, 2757–2767.
(21) Qureshi, A.; MacLeod, M.; Hungerbuhler, K. Quantifying uncertainties in the global mass balance of mercury. *Glob. Biogeochem Cycles* **2011**, *25*, GB4012.
(22) Galarneau, E.; Makar, P. A.; Zheng, Q.; Narayan, J.; Zhang, J.; Moran, M. D.; Bari, M. A.; Pathela, S.; Chen, A.; Chlumsky, R. PAH concentrations simulated with the AURAMS-PAH chemical transport model over Canada and the USA. *Atmos Chem Phys* **2014**, *14*, 4065–4077.
(23) Friedman, C. L.; Pierce, J. R.; Selin, N. E. Assessing the influence of secondary organic verus primary carbonaceous aerosols on long-range atmospheric polycyclic aromatic hydrocarbon transport. *Env. Sci Technol* **2014**, *48* (6), 3293–3302.
(24) Wohrnschimmel, H.; MacLeod, M.; Hungerbuhler, K. Emissions, Fate and Transport of Persistent Organic Pollutants to the Arctic in a Changing Global Climate. *Env. Sci Technol* **2013**, *47*, 2323–2330.
(25) Phenix, B. D.; Dinaro, J. L.; Tatang, M. A.; Tester, J. W.; Howard, J. B.; McRae, G. J. Incorporation of parametric uncertainty into complex kinetic mechanisms: Application to hydrogen oxidation in supercritical water. *Combust. Flame* **1998**, *112* (1–2), 132–146.
(26) Isukapalli, S. S.; Balakrishnan, S.; Georgopoulos, P. G. Computationally efficient uncertainty propagation and reduction using the stochastic response surface method. In *43rd IEEE Conference on Decision and Control, 2004. CDC*; 2004; Vol. 2, pp 2237–2243 Vol.2.
(27) Lucas, D. D.; Prinn, R. G. Parametric sensitivity and uncertainty analysis of dimethylsulfide oxidation in the clear-sky remote marine boundary layer. *Atmos Chem Phys* **2005**, *5* (6), 1505–1525.
(28) Cheng, H.; Sandu, A. Uncertainty quantification and apportionment in air quality models using the polynomial chaos method. *Environ. Model. Softw.* **2009**, *24* (8), 917–925.
(29) Dachs, J.; Eisenreich, S. J. Adsorption onto aerosol soot carbon dominates gas-particle partitioning of polycyclic aromatic hydrocarbons. *Env. Sci Technol* **2000**, *34*, 3690–3697.
(30) Bond, T. C.; Bhardwaj, E.; Dong, R.; Jogani, R.; Jung, S.; Roden, C.; Streets, D. G.; Trautmann, N. M. Historical emissions of black and organic carbon aerosol from energy-related combustion, 1850-2000. *Glob. Biogeochem Cycles* **2007**, *21*, GB2018.
(31) Bey, I.; Jacob, D. J.; Yantosca, R. M.; Logan, J. A.; Field, B.; Fiore, A. M.; Li, Q.; Liu, H.

X.; Mickley, L. J.; Schultz, M. Global modeling of tropospheric chemistry with assimilated meteorology: Model description and evaluation. *J Geophys Res* **2001**, *106*, 23,073–23,096.

(32) Kahan, T. F.; Kwamena, N.-O. A.; Donaldson, D. J. Heterogeneous ozonation kinetics of polycyclic aromatic hydrocarbons on organic films. *Atmos Env.* **2006**, *40*, 3448–3459.

(33) Wang, Y.; Jacob, D.; Logan, J. Global simulation of tropospheric O3-NOx-hydrocarbon chemistry: 1. Model formulation. *J Geophys Res* **1998**, *103(D9)*, 10,713–10,725.

(34) Tatang, M. A.; Pan, W.; Prinn, R. G.; McRae, G. J. An efficient method for parametric uncertainty analysis of numerical geophysical models. *J. Geophys. Res. Atmospheres* **1997**, *102* (D18), 21925–21932.

(35) Barring, H.; Bucheli, T. D.; Broman, D.; Gustafsson, O. Soot-water distribution coefficients for polychlorinated dibenzo-p-dioxins, polychlorinated dibenzofurans and polybrominated diphenylethers determined with the soot cosolvency-column method. *Chemosphere* **2002**, *49* (6), 515–523.

(36) Kwok, E. S. C.; Harger, W. P.; Arey, J.; Atkinson, R. Reactions of Gas-Phase Phenanthrene under Simulated Atmospheric Conditions. *Environ. Sci. Technol.* **1994**, *28* (3), 521–527.

(37) Atkinson, R. Kinetics and mechanisms of the gas-phase reactions of the hydroxyl radical with organic compounds. *J Phys Chem Ref Data* **1989**, *Monograph 1*, 1–246.

(38) Biermann, H. W.; Mac Leod, H.; Atkinson, R.; Winer, A. M.; Pitts, J. N. Kinetics of the gas-phase reactions of the hydroxyl radical with naphthalene, phenanthrene, and anthracene. *Env. Sci Technol* **1985**, *19*, 244–248.

(39) Benzo[a]pyrene http://webbook.nist.gov/cgi/cbook.cgi?ID=C50328&Mask=20 (accessed Jun 29, 2014).

(40) Kazakov, S. M.; Kaputerko, M. N.; Suchkov, V. A. Determination of first ionization potentials from spectra of electronic energy loss in the vapor of polyatomic organic compounds. *J. Appl. Spectrosc.* **1999**, *66* (3), 375–379.

(41) Chen, Y.-H.; Prinn, R. G. Estimation of atmospheric methane emissions between 1996 and 2001 using a three-dimensional global chemical transport model. *J Geophys Res* **2006**, *111* (D10), 27.

(42) Hung, H.; MacLeod, M.; Guardans, R.; Scheringer, M.; Barra, R.; Harner, T.; Zhang, G. Toward the next generation of air quality monitoring: Persistent organic pollutants. *Atmos Env.* **2013**, *80*, 591–598.

(43) Goss, K.-U. Comment on "Influence of Soot Carbon on the Soil-Air Partitioning of Polycyclic Aromatic Hydrocarbon." *Env. Sci Technol* **2004**, *38* (5), 1622–1623.

(44) Liu, H.; Jacob, D. J.; Bey, I.; Yantosca, R. M. Constraints from 210Pb and 7Be on wet deposition and transport in a global three-dimensional chemical tracer model driven by assimilated meteorological fields. *J Geophys Res* **2001**, *106(D11)*, 12,109–112,128.

(45) Wu, S.; Mickley, L. J.; Jacob, D. J.; Logan, J. A.; Yantosca, R. M.; Rind, D. Why are there large differences between models in global budgets of tropospheric ozone? *J Geophys Res* **2007**, *112* (D05302).

(46) Shindell, D. T.; Chin, M.; Dentener, F.; Doherty, R. M.; Faluvegi, G.; Fiore, A. M.; Hess, P.; Koch, D. M.; MacKenzie, I. A.; Sanderson, M. G.; et al. A multi-model assessment of pollution transport to the Arctic. *Atmos Chem Phys* **2008**, *8*, 5353–5372.

646

647 **Table 1. Uncertainty of physicochemical properties in GEOS-Chem PAH simulations**
648 **(means and standard deviations of normal distributions).**

Parameter	Role	BaP Value (std.)	PYR Value (std.)	PHE Value (std.)
$\log_{10} K_{BC\text{-}Water}$ (unitless)	BC partition coefficient	8.8 (0.4)	7.5 (0.2)	6.85 (0.3)
$\log_{10} K_{OA}$ (unitless)	OC partition coefficient	11.27 (0.21)	8.78 (0.08)	7.58 (0.06)
ΔH_{vap} (kJ/mol)	Enthalpy of vaporization	99.9 (7.4)	82.3 (3.9)	68.3 (8.9)
$\log_{10} K_{AW}$ (unitless)	Air-water partition coefficient	-4.42 (0.08)	-3.34 (0.07)	-2.81 (0.06)
ΔH_{sol} (kJ/mol)	Enthalpy of solvation	37.9 (17.7)	37.9 (8.9)	34.5 (2.0)
k_{OH} (cm^3 $molec^{-1}$ s^{-1}) ($\log_{10} k_{OH}$ for BaP and PYR)	Gas-phase oxidation rate constant	-9.88 (0.26) ($\log_{10} k_{OH}$)	-10.1 (0.35) ($\log_{10} k_{OH}$)	1.9×10^{-11} (0.4×10^{-11})
k_{O3} (10^{-7} s^{-1}, at 50ppb O_3)	On-particle oxidation rate constant	24.5 (3.5)	2.92 (1.21)	2.91 (0.92)

649

650

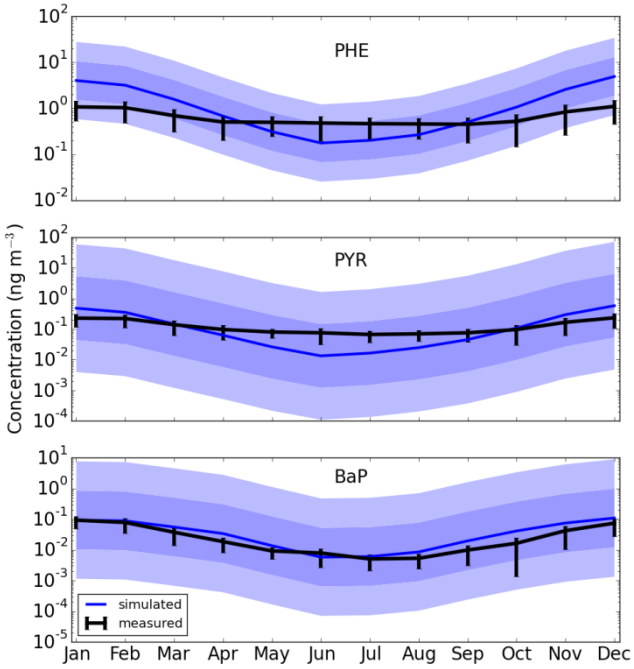

Figure 1. Measured and simulated total (gas and particulate) concentrations at non-urban sites for PHE (top), PYR (middle), and BaP (bottom). The black lines are means across the measurements at all non-urban sites, and their error bars show the standard deviation of the mean for each month. The blue lines are the simulated means across the same sites, with the shaded regions marking the σ and 2σ intervals of the parametric uncertainty distributions for each month.

(a) PHE

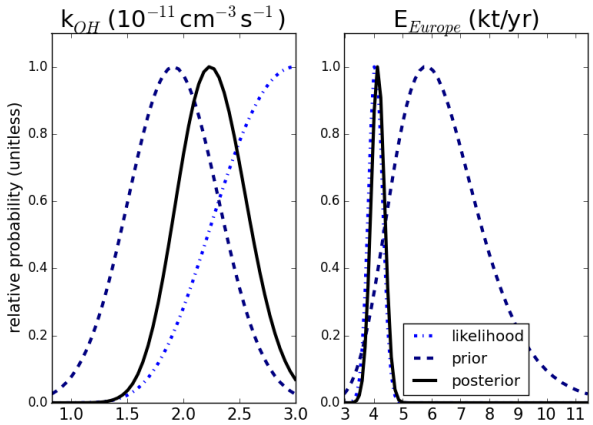

(b) PYR

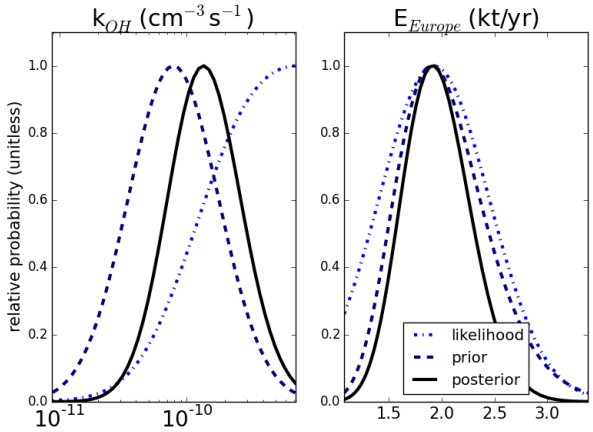

(c) BaP

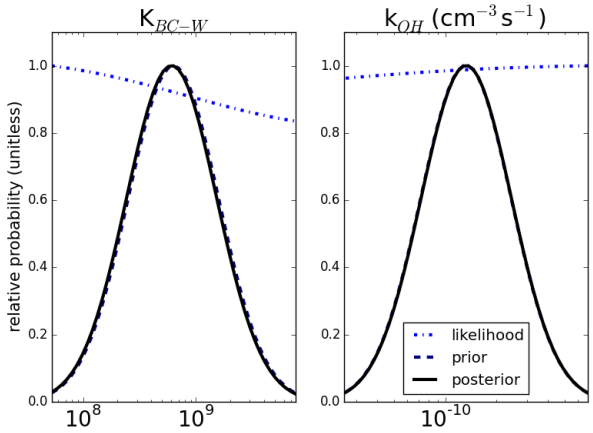

Figure 2. Constraint of parameter uncertainty distributions by measurement data. (a) PHE, (b) PYR, (c) BaP distributions for the two most important parameters each. Prior distributions (dashed lines), observation-based likelihoods (dot-dashed lines), and posterior distributions (solid lines) shown.